JACC: BASIC TO TRANSLATIONAL SCIENCE
VOL. 1, NO. 4, 2016
ISSN 2452-302X
http://dx.doi.org/10.1016/j.jacbts.2016.04.005

PRE-CLINICAL RESEARCH

Chemotherapeutic Efficacy of Phosphodiesterase Inhibitors in Chagasic Cardiomyopathy

Jian-jun Wen, PhD,[a] Xianxiu Wan, MS,[a] John Thacker, BS,[a] Nisha Jain Garg, PhD[a,b,c]

VISUAL ABSTRACT

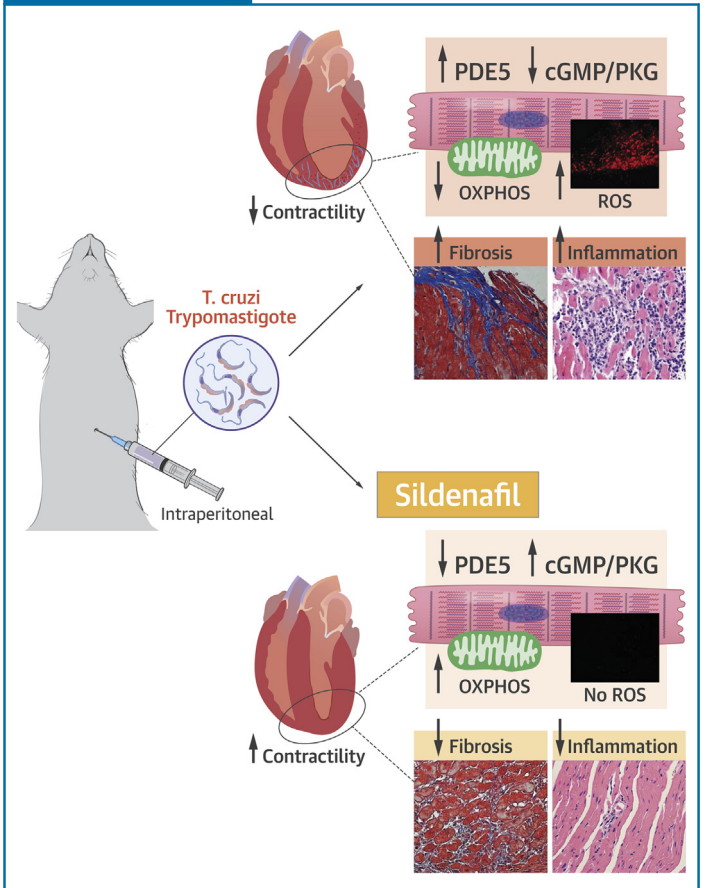

Wen, J.-j. et al. J Am Coll Cardiol Basic Trans Science. 2016;1(4):235–50.

HIGHLIGHTS

- Mice infected with *T. cruzi* control acute parasitemia but develop chronic chagasic cardiomyopathy.
- Treatment with SIL (a phosphodiesterase inhibitor) during a therapeutic window of indeterminate phase provided powerful cardioprotective effects against chronic development of cardiomyopathy and LV dysfunction.
- SIL normalized the cGMP-dependent protein kinase activity and mitochondrial oxidative metabolism, and established the oxidant/antioxidant balance in chagasic myocardium.
- SIL prevented the oxidative/inflammatory adducts that precipitate cardiomyocytes death and cardiac remodeling in CCM.

From the [a]Department of Microbiology and Immunology, University of Texas Medical Branch, Galveston, Texas; [b]Department of Pathology, University of Texas Medical Branch, Galveston, Texas; and the [c]Institute for Human Infections and Immunity, University of Texas Medical Branch, Galveston, Texas. This work was supported by a grant from the National Institute of Allergy and Infectious Diseases at National Institutes of Health (2RO1AI054578) to Dr. Garg. Ms. Wan is supported by a pre-doctoral fellowship from the American Heart Association and a fellowship from the McLaughlin Endowment at University of Texas Medical Branch. The authors have reported that they have no relationships relevant to the contents of this paper to disclose.

Manuscript received February 5, 2016; revised manuscript received April 11, 2016, accepted April 24, 2016.

JACC: BASIC TO TRANSLATIONAL SCIENCE VOL. 1, NO. 4, 2016
JUNE 2016:235–50

SUMMARY

Molecular mechanisms of *Trypanosoma cruzi* (*Tc*)-induced Chagasic cardiomyopathy (CCM) are not well understood. The NO-cGMP-PKG1α pathway maintains cardiac homeostasis and inotropy and may be disturbed due to phosphodiesterase (PDE5)-mediated cGMP catabolism in CCM. To test this, C57BL/6 mice were infected with *T. cruzi*, and after the control of acute parasitemia (~45 days post-infection), given sildenafil (SIL) (1 mg/kg) treatment for 3 weeks that ended long before the chronic disease phase (~150 days post-infection). The PDE5 was increased and cGMP/PKG activity was decreased in chagasic myocardium. Transthoracic echocardiography revealed left ventricular (LV) systolic function, that is, stroke volume, cardiac output, and ejection fraction, was significantly decreased in chagasic mice. SIL treatment resulted in normal levels of PDE5 and cGMP/PKG activity and preserved the LV function. The cardioprotective effects of SIL were provided through inhibition of cardiac collagenosis and chronic inflammation that otherwise were pronounced in CCM. Further, SIL treatment restored the mitochondrial DNA–encoded gene expression, complex I–dependent (but not complex II–dependent) ADP-coupled respiration, and oxidant/antioxidant balance in chagasic myocardium. In vitro studies in cardiomyocytes verified that SIL conserved the redox metabolic state and cellular health via maintaining the antioxidant status that otherwise was compromised in response to *T. cruzi* infection. We conclude that SIL therapy was useful in controlling the LV dysfunction and chronic pathology in CCM. (J Am Coll Cardiol Basic Trans Science 2016;1:235–50)

ABBREVIATIONS AND ACRONYMS

ANOVA = analysis of variance
CCM = chagasic cardiomyopathy
cGMP = cyclic guanosine monophosphate
C_t = threshold cycle
DCF = dichlorodihydrofluorescein
DHE = dihydroethidium
DMSO = dimethyl sulfoxide
EF = ejection fraction
ER = endoplasmic reticulum
GC = guanylyl cyclase
HRP = horseradish peroxidase
K-W = Kruskal-Wallis
LDH = lactate dehydrogenase
LPO = lipid hydroperoxide
LV = left ventricle/ventricular
mtDNA = mitochondrial DNA
NO = nitric oxide
OD = optical density
PDE = phosphodiesterase
pi = post-infection
PKG = cGMP-dependent protein kinase
QR1 = quartile 1
RCR = respiratory control ratio
ROS = reactive oxygen species
SIL = sildenafil
SV = stroke volume
Tc = *Trypanosoma cruzi*

Chagasic cardiomyopathy (CCM) is an illness initiated by *Trypanosoma cruzi* infection. In Latin America, ~13 million people are infected and 120 million are believed to be at risk of infection via vectorial, congenital, and other modes of transmission (1). Vectorial transmission occurs in the United States (2), and >300,000 infected individuals living in the United States can potentially transfer infection through blood and organ donation (3–5). Approximately, 30% to 40% of the infected individuals manifest prolonged micro and macro cardiac injuries that cause hypertrophy and increased stiffness of the left ventricular (LV) walls, and ultimately lead to a clinical presentation of ventricle arrhythmia, thromboembolism, and heart failure (6). Due to a lack of accurate therapies (7), CCM causes approximately $8 billion/year in costs in health care and loss of productivity (8).

Molecular mechanisms of *T. cruzi* (*Tc*)-induced CCM are not well understood. Early upon infection, *T. cruzi* is shown to upregulate in human cardiac myocytes the expression of several transcription factors and cytokines/chemokines implicated in the development of fibrogenic response (9). Chronic progression of CCM is associated with persistent increase in circulatory and myocardial inflammatory and oxidative stress in human patients and experimental models (reviewed in [10]). Although inflammatory stress is believed to be present in response to *T. cruzi* infection, we showed that mitochondrial inefficiency of respiratory chain was the major source of reactive oxygen species (ROS) in the heart (11). Treatment of chagasic mice with a ROS scavenger (12) and mice genetically enhanced in their capacity to scavenge mitochondrial ROS (13) were better equipped in handling the oxidative and inflammatory stress, thus suggesting that ROS may signal chronic inflammation during CCM.

In the heart, nitric oxide (NO) and atrial natriuretic peptide signal the activation of guanylyl cyclase (GC) that produces cyclic guanosine monophosphate (cGMP) (14). The cGMP binding activates cGMP-dependent protein kinase (PKG). PKG phosphorylates serine and threonine residues on many cellular proteins and mediates the downstream effects in maintaining the force of contraction of cardiac myocytes (15) through regulating cytosolic free Ca^{2+} level and sensitivity of muscle fibers to Ca^{2+} (16). Others have implied that cGMP/PKG regulate the activities of phosphodiesterases (PDEs) that hydrolyze cyclic nucleotides (17). Of the 4 PDEs that are expressed in the heart and, in a feedback mechanism, that hydrolyze cyclic nucleotides, PDE5 is the only known cardiac phosphodiesterase that selectively hydrolyzes cGMP and negatively regulates cardiac inotropy (18). An observation of PDE5 subcellular localization to myocyte z-bands (19) implies that it may exert its effects on cGMP/PKG signaling in a spatiotemporal manner and determine the functional outcomes in stressed heart. The NO-cGMP-PKG signaling may also occur in mitochondria and play a role in ischemic preconditioning and antioxidant cardioprotection (20), though the exact mechanism remains to be identified.

In this study, we aimed to determine whether treatment with PDE5 inhibitors would be beneficial in preserving cardiac hemodynamics in CCM. We also determined the molecular mechanism of cGMP/PKG in preventing pathological outcomes in CCM. We discuss the therapeutic role of PDE5 inhibitors in arresting the myocardial inflammation and mitochondrial oxidative stress that are hallmarks of chronic CCM.

MATERIALS AND METHODS

ETHICS STATEMENT. All animal experiments were performed according to the National Institutes of Health Guide for Care and Use of Experimental Animals, and was approved by the Institutional Animal Care and Use Committee at the University of Texas Medical Branch, Galveston (protocol number: 805029).

MICE, PARASITES, AND CELL CULTURE. All experiments were conducted in C57BL/6 (wild-type, female) mice, and all mice were purchased from Harlan Laboratories (Indianapolis, Indiana). *T. cruzi* trypomastigotes (SylvioX10/4) were propagated by in vitro passage in C2C12 cells. Mice were randomly assigned to different groups. Mice (6-weeks-old) were infected with *T. cruzi* (10,000 trypomastigotes/mouse, intraperitoneal), and survival from infection was monitored daily. Sildenafil (SIL) solution (25 μg/100 μl of 0.5% dimethyl sulfoxide [DMSO]) was freshly made, and treatment with SIL (1 mg/kg, intraperitoneal) was initiated at day 45 post-infection (pi) when mice had controlled acute parasitemia, and was conducted twice a week for 3 weeks. The selected low concentration of SIL was shown to be safe while providing cardiac benefits in previous studies (21). Mice were sacrificed at ~150 days pi corresponding to the chronic disease phase. Sera/plasma and tissue samples were stored at 4°C and −80°C, respectively.

PKG ACTIVITY. A CycLex cGK (PKG) ELISA Assay Kit (MBL International Corp, Woburn, Massachusetts) was used to measure the PKG activity. Briefly, tissue homogenates (10-μg protein/10 μl) were added to 96-well plates pre-coated with histone H1 peptide containing threonine residues, and sequentially incubated for 30 min in the presence of cGMP and ATP, and then for 60 min with horseradish peroxidase (HRP)-conjugated anti-phospho-G-kinase substrate threonine 68/119 monoclonal antibody. Plates were washed, and the HRP-catalyzed conversion of chromogenic TMB substrate to a blue color was recorded at 450/540 nm (standard curve 1- to 10-U recombinant cGK [PKG] protein).

ECHOCARDIOGRAPHY. Mice were sedated with inhalant anesthesia (1.5% isoflurane/100% O_2), placed supine on an electrical heating pad at 37°C, and heart rate and respiratory physiology were continuously monitored by electrocardiography. After shaving the chest, warmed ultrasound gel was applied, and transthoracic echocardiography was performed using the Vevo 2100 ultrasound system (VisualSonics, Toronto, Canada) equipped with a high-frequency linear array transducer (MS400, 18 to 38 MHz) (22). Heart was imaged in B-mode and M-mode to examine the parameters of the left ventricle (LV) in diastole and systole. All measurements were obtained in triplicate, and data were analyzed using the Vevo 2100 standard measurement package.

HISTOLOGY. Tissue sections were fixed in 10% buffered formalin for 24 h, dehydrated in absolute ethanol, cleared in xylene, and embedded in paraffin. Five-micron tissue sections were subjected to staining with hematoxylin and eosin or Mason's Trichrome at the Research Histopathology Core at the University of Texas Medical Branch, and evaluated by light microscopy using an Olympus BX-15 microscope (Center Valley, Pennsylvania) equipped with a digital camera and Simple PCI software (v.6.0; Compix, Sewickley, Pennsylvania). Myocarditis (presence of inflammatory cells) in hematoxylin and eosin-stained tissue sections was scored as 0 (absent), 1 (focal/mild, ≤1 foci), 2 (moderate, ≥2 inflammatory foci), 3 (extensive, coalescing of inflammatory foci or disseminated inflammation), and 4 (diffused inflammation, tissue necrosis, interstitial edema, and loss of integrity). Inflammatory infiltrates were characterized as diffused or focal depending upon how closely the inflammatory cells were associated (23). Fibrosis was assessed by measuring the collagen area as a percentage of the total myocardial area, and categorized as 0 (<1%), 1 (1% to 5%), 2 (5% to 10%), 3 (10% to 15%), and 4 (>15%) on the basis of percent fibrotic area (23).

GENE EXPRESSION ANALYSIS. Heart tissue-sections (10 mg) were homogenized in 100 μl of TRIzol reagent (Invitrogen, Carlsbad, California), and total RNA was extracted and precipitated by the chloroform/isopropanol/ethanol method. DNA that might be contaminating the RNA preparation was removed by RNase-Free DNase I (New England Biolabs, Beverly, Massachusetts) treatment. Total RNA was analyzed by using a DU 800 UV/Visible Spectrophotometer (Beckman Coulter, Pasadena, California) and absorbance read at 260 nm and 280 nm to assess the quality (optical density $[OD]_{260}/OD_{280}$ ratio ≥2.0) and quantity (OD_{260} of 1 = 40 μg/ml RNA). An aliquot of total RNA was run on a 1.5% denaturing agarose gel to assess the integrity (28S/18S, 2:1 ratio). Total RNA (2 μg) was reverse transcribed with $Oligo(dT)_{20}$ primer using SuperScript III Reverse Transcriptase (Invitrogen). The cDNA was used as a template in a

real-time quantitative polymerase chain reaction on an iCycler Thermal Cycler with SYBR-Green Supermix (Bio-Rad, Hercules, California) and gene-specific oligonucleotides (Table 1). The threshold cycle (C_t) values for target mRNAs were normalized to *GAPDH* mRNA, and the relative expression level of each target gene was calculated as $2^{-\Delta\Delta Ct}$, where ΔC_t represents the C_t (sample) − C_t (control). The fold change represents (the target $2^{-\Delta\Delta Ct}$ / the control $2^{-\Delta\Delta Ct}$) (12).

WESTERN BLOTTING. Freshly harvested heart tissues were minced in ice-cold HMSB medium (10 mmol/l HEPES [pH 7.4], 225 mmol/l mannitol, 75 mmol/l sucrose, and 0.2% fatty acid-free bovine serum albumin; tissue/buffer ratio, 1:20), homogenized in a Dounce homogenizer, and centrifuged at 600 *g* to pellet the debris. Heart homogenates (20 μg of protein) were electrophoresed on a 10% Mini-Protein TGX gel using a Mini-PROTEAN electrophoresis chamber (Bio-Rad), and proteins were transferred to a polyvinylidene difluoride membrane using a semidry transfer system (Bio-Rad). Membranes were blocked with 5% nonfat dry milk in 50 mmol/l Tris-HCl (pH 7.5)/150 mmol/l NaCl (TBS), washed with TBS-0.1% Tween 20, and incubated overnight at 4°C with antibodies against PDE5 (cat# ab14672; Abcam, San Francisco California) and GAPDH (cat#3683; Cell Signaling Technology, Danvers, Massachusetts). Membranes were incubated with HRP-conjugated secondary antibody (1:5,000 dilution, cat# 4041-05; Southern Biotech, Birmingham Alabama), and signal was captured by using an ImageQuant LAS4000 system (GE Healthcare, Pittsburgh, Massachusetts). Densitometry analysis of protein bands of interest was performed using a Fluorchem HD2 Imaging System (Alpha-Innotech, San Leandro, California), and normalized against GAPDH.

LACTATE DEHYDROGENASE. Lactate dehydrogenase (LDH) activity in tissue homogenates and plasma was measured by using a 2-step kit (Cayman Chemicals, Ann Arbor, Michigan). Briefly, LDH-catalyzed reduction of NAD^+ to NADH by oxidation of lactate to pyruvate was coupled with reduction of tetrazolium salt to blue formazan crystals, and absorbance was monitored at 490 to 520 nm by spectrophotometry (standard curve 1 to 1,000 μU of LDH).

TISSUE PARASITE BURDEN. Heart tissues were harvested from normal, *Tc*-infected, and *Tc*-infected/SIL-treated mice as described earlier in the text. A batch of *Tc*-infected mice were injected with DMSO (0.5%, 100 μl per mouse, vehicle for dissolving SIL) and used to evaluate the potential effect of DMSO on parasite burden. Tissue sections (10 mg) were subjected to proteinase-K lysis, and total DNA was extracted by the phenol/chloroform extraction/ethanol precipitation method. Total DNA was treated with RNase A (DNase and protease-free, cat#EN0531, Thermo Fisher Scientific, Waltham, Massachusetts) and purified by using DNeasy Mini Spin Columns (Qiagen, Hilden, Germany). Total DNA absorbance was recorded at 260 and 280 nm by using a DU 800 UV/Visible Spectrophotometer, and DNA concentration ($[OD_{260} - OD_{320}] \times 50$ μg/ml) and purity (OD_{260}/OD_{280} ratio of 1.7 to 2.0) recorded. Total DNA (100 ng) was submitted to a real-time polymerase chain reaction on an iCycler thermal cycler with SYBR Green Supermix (Bio-Rad) and *Tc*18SrDNA-specific primers (forward: 5′-TAGTCATATGCTTGTTTC-3′, reverse: 5′-GCAACAGCATTAATATACGC-3′), and fold change was calculated as described earlier in the text.

MITOCHONDRIAL RESPIRATION. Freshly harvested tissue sections (30 mg) were minced in 500 μl of ice-cold HMSB medium (10 mmol/l HEPES pH 7.4,

TABLE 1 Oligonucleotides Used in the Study

Gene	5′-Forward-3′	5′-Reverse-3′	Amplicon Size (bp)	Accession #
ATP6	CCTTCCACAAGGAACTCCA	GGTAGCTGTTGGTGGGCTAAA	195	NC_005089
Collagen I	GAGCGGAGAGTACTGGATCG	GCTTCTTTTCCTTGGGGTTC	158	BC050014
Collagen III	GCACAGCAGTCCAACGTAGA	TCTCCAAATGGGATCTCTGG	185	BC058724
COXIII	CCTTCGACCTGACAGAAGGA	GATGCTCGGATCCATAGGAA	238	DQ106413.1
Cyt B	ATTCCTTCATGTCGGACGAG	ACTGAGAAGCCCCCTCAAAT	228	GI325511952
GAPDH	AACTTTGGCATTGTGGAAGG	ACACATTGGGGGTAGGAACA	223	NM_008084.2
GSK3β	CAGTGGTGTGGATCAGTTGG	ATGTGCACAAGCTTCCAGTG	232	NM_019827.6
MnSOD	CACATTAACGCGCAGATCATG	CCAGAGCCTCGTGGTACTTCTC	79	NM_013671.3
ND1	CTGGCTACTGCGTACATCCA	TCTCCAAACCCTTTGACACA	142	NM_004541.3
ND4	AGGACTTCCACATGGAGATTGGCA	AGACTGCATGTTATTGCGAGCAGG	162	NM_002495.2
PDE5	GGAAGCGTGGCTGGATGATCAC	AAGAGCAGGACTCGGTATGGGC	152	NM_153422.2
SERCA2	CTGTGGAGACCCTTGGTTGT	CAGAGCACAGATGGTGGCTA	145	NR_027838.1

bp = base pairs.

225 mmol/l mannitol, 75 mmol/l sucrose, and 0.2% fatty acid-free bovine serum albumin) containing 200 U/ml collagenase and homogenized on ice using a Dounce homogenizer. Collagenolysis was stopped with addition of 1 mmol/l EGTA, and tissue homogenates were centrifuged at 4°C for 10 min each at 600 g (to remove debris) and 8,000 g to pellet the mitochondrial fraction (24).

Mitochondrial respiration was measured by using a Mitocell S200A Respirometry System (Strathkelvin, Motherwell, United Kingdom). Briefly, a microcathode oxygen electrode was calibrated, and freshly isolated mitochondria (200 μg) suspended in 0.5 ml of MSP buffer (225 mmol/l mannitol, 75 mmol/l sucrose, 20 mmol/l KH_2PO_4/K_2HPO_4 [pH 7.6]) were added to the Mitocell. After recording the basal O_2 consumption, 230 μmol/l ADP was added, allowing the ATP synthase to function and complex I (10 mmol/l pyruvate/10 mmol/l glutamate/2.5 mmol/l malate) or complex II (5 mmol/l succinate/6.25 μmol/l rotenone) coupled state 3 respiration (indicates ATP production rate) was recorded (24).

OXIDATIVE STRESS. The in situ ROS level was measured in cryostat sections. Tissue sections (10 μm) were equilibrated in Kreb's buffer and incubated in the dark for 30 min with 5 μmol/l MitoSOX Red (Invitrogen). MitoSOX Red oxidation by mitochondrial ROS, resulting in red fluorescence (Ex_{518nm}/Em_{605nm}), was detected on an Olympus BX-15 microscope and images were captured by using a mounted digital camera.

We used an LPO Assay Kit (Cayman Chemicals) to measure the lipid peroxides. Briefly, lipid hydroperoxide (LPO) in tissue homogenates or plasma samples were extracted into chloroform, and added to 50 μl of 4.5 mmol/l $FeSO_4$ in 0.2 mol/l HCl / 3% NH_4SCN in methanol (1:1, v/v). The redox reaction with ferrous ions was stopped after 5 min, and absorbance was monitored at 500 nm (standard curve 0 to 500 μmol/l 13-hydroperoxy octadecadienoic acid).

The protein carbonyls in tissue homogenates were measured by a colorimetric protein carbonyl assay (Cayman Chemicals), according to the instructions provided by the manufacturer.

ROS release by *Tc*-infected cells (±SIL) was measured by an Amplex red assay. Briefly, samples (10 μg of protein) were added in triplicate to 96-well, black, flat-bottom plates. The reaction was initiated with addition of 50 μl each of 100 μmol/l Amplex red (Invitrogen) and 0.3 U/ml HRP. The HRP-catalyzed Amplex red oxidation by H_2O_2, resulting in fluorescent resorufin formation, was monitored at $Ex_{563\ nm}/Em_{587\ nm}$ (standard curve 50 nmol/l – 5 mol/l H_2O_2).

ANTIOXIDANT LEVELS. MnSOD activity in tissue homogenates was measured using a Superoxide Dismutase Assay kit (Cayman Chemicals). The assay uses a tetrazolium salt for detection of superoxide radicals generated by xanthine oxidase and hypoxanthine. One unit of SOD was defined as the amount of MnSOD needed for 50% dismutation of the superoxide radical (standard curve 0.005 to 0.05 U/ml recombinant CuZnSOD).

Total antioxidant capacity was assessed using lag time by antioxidants against the myoglobin-induced oxidation of 2,2'-azino-di(3-ethylbenzthiazoline-6-sulfonic acid (ABTS) with H_2O_2. Briefly, 20 μl of plasma samples (diluted 1:20, v/v) were added in triplicate to 96-well plates, and mixed with 90 μl of 10 mmol/l PBS (pH 7.2), 50 μl of myoglobin solution, and 20 μl of 3 mmol/l ABTS. Reaction was initiated with H_2O_2 (20 μl), and change in color was monitored at 600 nm (standard curve 2 to 25 μmol/l trolox).

FLUORESCENCE MICROSCOPY, NAD^+/NADH RATIO, CELL VIABILITY, AND TRANSIENT TRANSFECTION. Cultured cardiac myocytes (10^5 cells/well in 24-well plates) were infected with *T. cruzi* (cell/parasite ratio, 1:5) and incubated in presence or absence of 100 nmol/l SIL for 24 h. Cells were loaded for 30 min with 50 μl of cell permeable dyes (Molecular Probes, Eugene, Oregon), washed, and then the change in intracellular fluorescence was visualized and recorded by using an ECLIPSE Ti inverted microscope equipped with a digital camera (magnification 40×). The 2',7'-bis-(2-carboxyethyl)-5-(and-6)-carboxyfluorescein (BCECF acid, 2 to 10 μmol/l, Ex_{490nm}/Em_{535nm}) was used as a dual-excitation ratiometric indicator of changes in intracellular pH. Fluo-4 AM (1 μmol/l, Ex_{485nm}/Em_{520nm}) was used to measure the changes in intracellular Ca^{2+} concentrations in response to *Tc* infection. Cells were also loaded with 100 μmol/l dihydroethidium (DHE) or 10 μmol/l CM-H_2DCF-DA, and the formation of fluorescent ethidium (Ex_{498nm}/Em_{598nm}, detects intracellular $O_2^{\bullet-}$) and dichlorodihydrofluorescein (DCF) (Ex_{498nm}/Em_{598nm}, detects intracellular H_2O_2), respectively, were monitored by fluorescence microscopy.

To evaluate the cell viability, HeLa cells (1×10^4/well) were seeded in 96-well plates, and infected and incubated with or without SIL for 24 h, as described earlier in the text. Cells were washed, replenished with fresh medium (100 μl), loaded with 20 μl of MTT solution (5 mg/ml of 3-[4,5-dimethylthiazol-2-yl]-2,5-diphenyltetrazolium bromide), and incubated for 4 h. The MTT is metabolized by NAD(P)H-dependent cellular oxidoreductases, resulting in the formation of insoluble blue formazan crystals. Formazan crystals were dissolved in 100 μl of DMSO, and the

absorbance was recorded at 490 nm with a reference wavelength of 620 nm.

The NAD^+/NADH ratio was measured by using a Fluorometric Assay Kit (Abcam, Cambridge, United Kingdom) according to instructions provided by the manufacturer. Briefly, tissue homogenates were deproteinized with 1 mol/l perchloric acid, neutralized with equal volume of ice-cold 2 mol/l KOH, and centrifuged to obtain clear supernatant. Samples (50 μl/well) were added in triplicate to a 96-well plate, and NADH formation in the presence of 100 μl of NAD cycling mix and 10 μl of NADH developer was recorded. A standard curve was prepared using 1 to 100 pmol/l NADH, and NAD^+/NADH ratio in samples calculated as (NAD_{total} − NADH) / NADH.

The eukaryotic plasmids pBI.EGFP and pBI.EGFP-MnSOD (express full-length MnSOD, from Addgene, Cambridge, Massachusetts) (25) were transformed into *Escherichia coli* DH5 competent cells, grown in L-broth containing appropriate antibiotics (100 μg/ml), and purified using the Plasmid DNA Maxi Prep kit (Qiagen). Cultured cardiac myocytes were seeded (10^4 cells/well) in Lab-Tek II 8-well chamber slides (Nunc, Rochester, New York) and incubated overnight at 37°C, 5% CO_2 in antibiotic-free Opti-MEM medium. Cells were transfected with pBI.EGFP or pBI.EGFP-MnSOD (100 ng) by using Lipofectamine 2000 reagent (Invitrogen) following the instructions provided by the manufacturer; and 6 h after transfection, cells were visualized by optical and fluorescence microscopy. The number of total and GFP^+ cells were counted per microscopic field (10 fields per slide), and transfection efficiency was evaluated ([GFP^+ × 100] / total cells). After 6 h of incubation, cells were washed, replenished with complete medium for 3 to 5 h, infected with *T. cruzi* (cell/parasite ratio, 1:5), and incubated with or without 100 nmol/l SIL for 24 h. The relative EGFP-conjugated MnSOD expression was detected by fluorescence microscopy.

DATA ANALYSIS. Mice were randomly assigned to 3 groups (no treatment, *T. cruzi* infection, or *T. cruzi* infection followed by SIL treatment, n ≥ 6 mice per group per experiment). All experiments were conducted in 2 sets of mice per group, with triplicate observations per sample. Data were expressed as mean ± SEM. All data were analyzed using GraphPad Prism 5 software (version 5.04) (GraphPad Software, La Jolla, California). Data (linear range or log_{10} transformed) were analyzed by the Kolmogorov-Smirnov test to determine whether the data are normally distributed. Normally distributed data were analyzed by 1-way analysis of variance (ANOVA) with post-hoc Tukey test. If data were not normally distributed, then Kruskal-Wallis (K-W) with Dunn tests were used, and median ± quartile 1 (QR1) values were also calculated. Significance is presented by *Tc-infected versus normal or $^{\#}Tc$-infected versus Tc/SIL-treated ($^{*,\#}p < 0.05$, $^{**,\#\#}p < 0.01$, $^{***,\#\#\#}p < 0.001$).

RESULTS

We used a well-established experimental model (26) to assess the role of PDE5 inhibition in control of CCM. C57BL/6 mice were infected with *T. cruzi*, and treated with SIL at the end of acute parasitemia. Mice were assessed for cardiac pathology in the chronic disease phase (150 days pi).

The cGMP/PKG signals the contraction and relaxation of vascular smooth muscle cells and cardiac myocytes, and PDE5 may contribute to stress, for example, pressure overload, induced cardiac remodeling (18). We, therefore, first determined whether PKG/PDE5 imbalance contributes to disturbed LV systolic function and cardiac remodeling in chagasic disease. The PKG activity was decreased by 2.1-fold and PDE5 expression was increased by >1.4-fold at the mRNA level and by 110% at the protein level in the myocardium of chagasic (vs. normal) mice (**Figure 1A, a–d**) (all $^{*}p < 0.001_{ANOVA/Tukey}$). Transthoracic echocardiography was performed to evaluate the LV function in *Tc*-infected (±SIL) mice). Our data showed that stroke volume (SV), cardiac output, and ejection fraction (EF) were decreased by 55%, 52%, and 42%, respectively, in chronically infected/untreated mice (**Figure 1B, a–c**) (all $^{*}p < 0.001_{K\text{-}W/Dunn}$). SIL treatment resulted in normal levels of PKG activity and PDE5 expression in the myocardium of chagasic mice (**Figure 1A, a–d**) (all $^{\#}p < 0.001_{ANOVA/Tukey}$), and subsequently, LV systolic function (SV, cardiac output, EF) was preserved in chagasic/SIL-treated mice, when compared with that noted in infected/untreated mice (**Figures 1A and 1B, a–c**) (all $^{\#}p < 0.001_{K\text{-}W/Dunn}$). SIL-treated mice also exhibited normal levels of fractional shortening and LV posterior wall thickness that were decreased by 62.3% and 40.5%, respectively, in *Tc*-infected mice (**Figure 1B, d–e**) (all $^{*,\#}p < 0.001_{K\text{-}W/Dunn}$). The significant improvement in LV function and dimensions in *Tc*-infected/SIL-treated mice were also observed when median ± QR1 values were calculated (SV [μl]: 35.34 ± 9.01, 15.63 ± 3.32**, 35.25 ± 7.95$^{\#\#\#}$; % fractional shortening 32.22 ± 8.99, 13.28 ± 6.55***, 40.34 ± 13.32$^{\#\#\#}$; and LV posterior wall thickness [mm] 0.97 ± 0.48, 0.51 ± 0.40*, 1.25 ± 0.44$^{\#\#\#}$; normal, *Tc*-infected, *Tc*-infected/SIL-treated, respectively, $^{*,\#}p < 0.5_{K\text{-}W/Dunn}$).

Histological and molecular analysis of the myocardium showed the collagen deposits were increased by

FIGURE 1 SIL Controlled LV Dysfunction and Cardiac Remodeling in Chagasic Mice

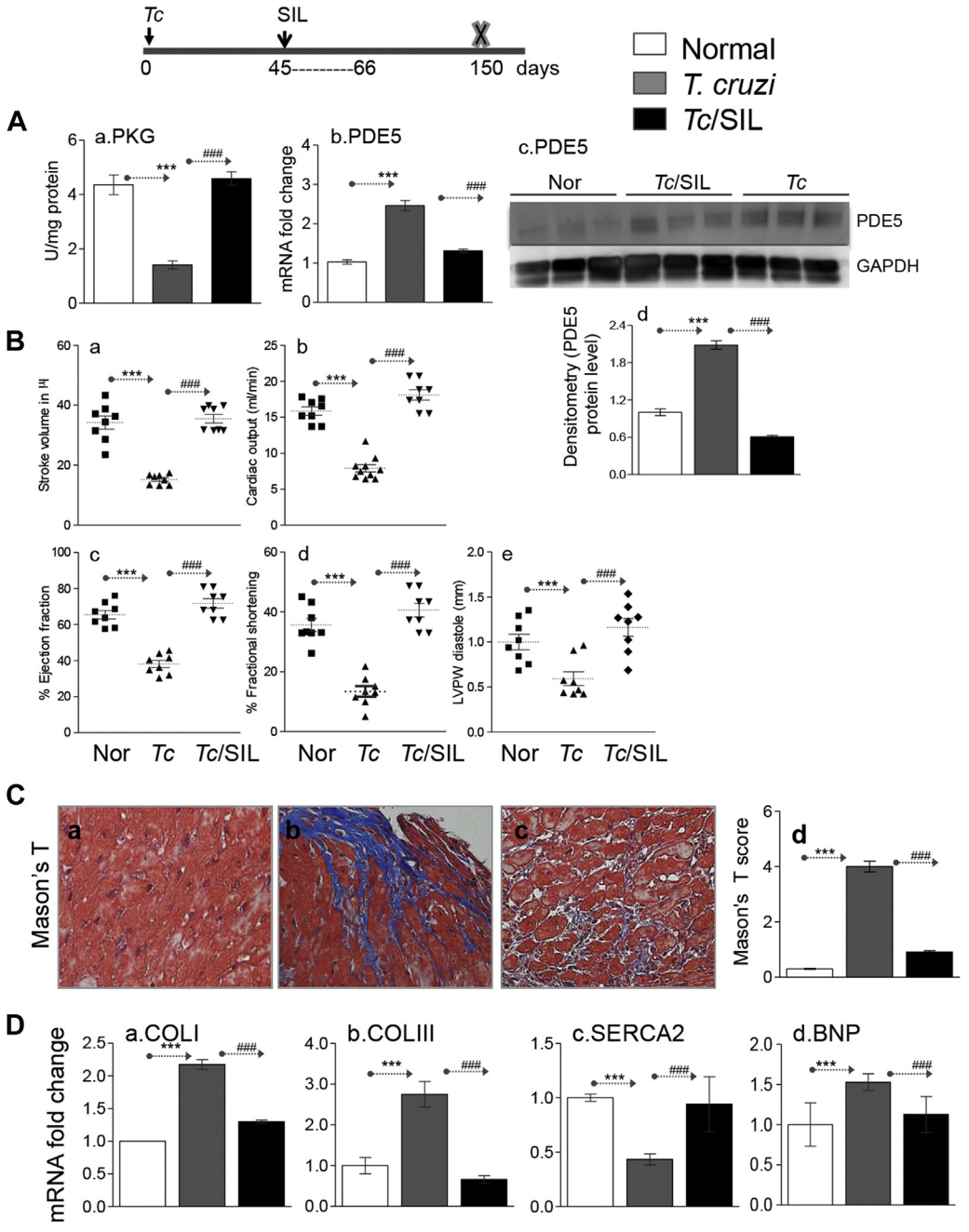

C57BL/6 mice were infected with *Trypanosoma cruzi* (*Tc*), and treated with sildenafil (SIL) for 3 weeks, beginning at day 45 post-infection (pi). Peripheral blood and heart tissues were collected at 150 days pi. **(A)** Shown are the myocardial levels of cGMP-dependent protein kinase activity (PKG) **(a)**, PDE5 mRNA by real-time quantitative reverse-transcription polymerase chain reaction (RT-PCR) **(b)**, and PDE5 protein level by Western blotting **(c)**. Densitometry units for PDE5 were normalized to GAPDH **(B)** transthoracic echocardiography was performed by using a Vevo 2100 System. Shown are **(a)** stroke volume, **(b)** cardiac output, **(c)** ejection fraction, **(d)** fractional shortening, and **(e)** left ventricular (LV) posterior wall thickness at diastole (LVPW). **(C)** Heart tissue sections were stained with Mason's Trichrome (**a–c**, magnification 20×), and scored for fibrosis **(d)** as described in Materials and Methods. **(D)** Quantitative RT-PCR analysis of mRNA levels for collagen isoforms *COLI* and *COLIII* **(a and b)** and *SERCA2* **(c)** in heart tissue of chronically infected (±SIL) mice. In all figures, data are plotted as mean ± SEM (n = 6 to 8 mice per group). Significance is shown with an **asterisk** (*Tc*-infected vs. matched control) or hash mark (infected/untreated vs. infected/SIL-treated), and presented as $^{*,\#}p < 0.05$, $^{**,\#\#}p < 0.01$, $^{***,\#\#\#}p < 0.001$. Mason's T = Mason's Trichrome; Nor = normal.

>12-fold (Figure 1C, b and d) (score 4.0 ± 0.392 vs. 0.3 ± 0.04, *$p < 0.001_{ANOVA/Tukey}$) and associated with 117% to 175% increase in collagen (*COLI and COLIII*) expression (Figure 1D, a and b) (*$p < 0.001_{ANOVA/Tukey}$) in chronically infected (vs. normal) mice. The *SERCA2* mRNA level was decreased by 131% in the myocardium of chagasic mice (Figure 1D, c) (*$p < 0.001_{ANOVA/Tukey}$). SIL treatment resulted in >90% control of *Tc*-induced collagen deposits and normalization of the expression levels of collagen (*COLI and COLIII*) and *SERCA2* mRNAs in the chagasic myocardium (Figures 1C and 1D) ($^{\#}p < 0.001_{ANOVA/Tukey}$). These data suggested that short-term treatment with SIL maintained the PDE5-PKG balance and provided cardioprotective effects through reversal (or inhibition) of adverse cardiac remodeling in chagasic mice.

Myocardial inflammatory response is important for control of acute infection, but its chronic persistence can contribute to cardiac tissue injury (27). PDE5 inhibitors may exert an anti-inflammatory effect by raising cGMP levels and thereby prevent cellular injuries in the heart. Histological studies showed extensive, diffused inflammatory infiltrate in the myocardium of chronically infected (vs. normal) mice (histological score 4.0 ± 0.39 vs. 0.3 ± 0.036, *$p < 0.01_{ANOVA/Tukey}$) (Figure 2A, a and b). Further, chronically infected mice exhibited a high degree of myocardial degeneration with enlarged myocytes. In comparison, minimal tissue inflammatory infiltrate (histological score 0.91 ± 0.12, $^{\#}p < 0.01_{ANOVA/Tukey}$) (Figure 2A, c) was detectable in chronically infected/SIL-treated mice. The myocardial and plasma levels of LDH (cellular injury marker) were increased by 5-fold and 55%, respectively, in infected/untreated (vs. normal) mice (Figure 2B, a and b) (all *$p < 0.001_{ANOVA/Tukey}$) but were maintained at normal levels in the SIL-treated/infected mice (Figure 2B, a and b) (all $^{\#}p < 0.001_{ANOVA/Tukey}$). The control of chronic inflammatory infiltrate and myocardial injury was observed despite the finding that tissue parasite burden was >2-fold higher in infected/SIL-treated mice, compared with that noted in infected/untreated mice (Figure 2C) ($^{\#}p < 0.001_{ANOVA/Tukey}$). These data suggested that SIL treatment was effective in controlling myocardial persistence of inflammatory infiltrate and tissue injury during chronic Chagas disease.

Mitochondrial activity of electron transport chain complexes is decreased in chagasic myocardium (28). To determine whether PDE5 contributes to mitochondrial dysfunction, we first performed quantitative evaluation of the mitochondrial DNA (mtDNA)-encoded gene expression in chagasic mice (±SIL). These data showed a coordinated decline (27% to 58%) in the expression of mtDNA-encoded genes that are essential for the assembly of functional complex 1 (*ND1* and *ND4*), complex III (*CYTB*), complex IV (*COXIII*), and complex V (*ATP6*) in cardiac biopsies of chagasic mice, when compared with that noted in normal mice (Figure 3A, a–e) (all *$p < 0.001_{ANOVA/Tukey}$). In infected mice given SIL treatment, the *ND1* mRNA level was preserved to normal level, and the expression of *CYTB* and *ATP6* was improved by 49% to 50% in comparison to that noted in chagasic/untreated mice (Figure 3A, a–e) (all $^{\#}p < 0.05$ to $0.001_{ANOVA/Tukey}$).

To determine whether SIL benefits in normalizing mtDNA gene expression influences the mitochondrial function, we assessed the oxygen consumption rate as a measure of mitochondrial oxidative metabolism in chagasic mice (± SIL). The ADP-coupled state 3 respiration (indicates proton gradient for ATP synthesis), driven with electron input from complex I (pyruvate + glutamate + malate) and complex II (succinate + rotenone) substrates, was decreased by 42% to 58% in isolated cardiac mitochondria of chagasic (vs. normal) mice (Figure 3B, a and b) (*$p < 0.001_{K\text{-}W/Dunn}$). Respiratory control ratio (RCR) (state 3/state 4, indicates mitochondrial integrity) was not disturbed in complex I respiring mitochondria from any of the *Tc*-infected mice, whereas complex II-driven RCR was decreased by 40% in cardiac mitochondria of *Tc*-infected mice (Figure 3B, c) (*$p < 0.001_{K\text{-}W/Dunn}$). SIL treatment arrested the loss in complex I-driven coupled respiration (Figure 3B, a) (median ± QR1: 41.37 ± 10.82, 15.29 ± 4.84***, 47.22 ± 32.98$^{\#\#\#}$ n mol/min/mg mitochondrial protein, normal, *Tc*-infected, *Tc*-infected/SIL-treated, respectively, $p < 0.001_{K\text{-}W/Dunn}$), but was not effective in improving the loss in complex II-driven coupled respiration and RCR in cardiac mitochondria of chagasic mice (Figure 3B, b and c). These data suggested that disease-associated compromise in mitochondrial biogenesis and function were controlled, at least partially, by SIL treatment of chagasic mice.

Because the loss in complex II-driven coupled respiration was not controlled in chagasic mice with SIL treatment, we expected that electron leakage from the respiratory chain would result in increased superoxide formation and oxidative stress in the infected myocardium. Indeed, myocardial staining with MitoSOX Red (detects mitochondrial ROS) was increased in chagasic (vs. normal) mice (Figure 4A, a and b). ROS action on polyunsaturated fatty acids results in the formation of highly reactive LPOs; and ROS-dependent direct oxidation of amino acids produces protein-derived aldehydes and ketones that are collectively termed as carbonyls (29). The myocardial and plasma levels of LPO and myocardial

FIGURE 2 **Effects of SIL on Myocardial Inflammation and Parasite Burden in Chagasic Mice**

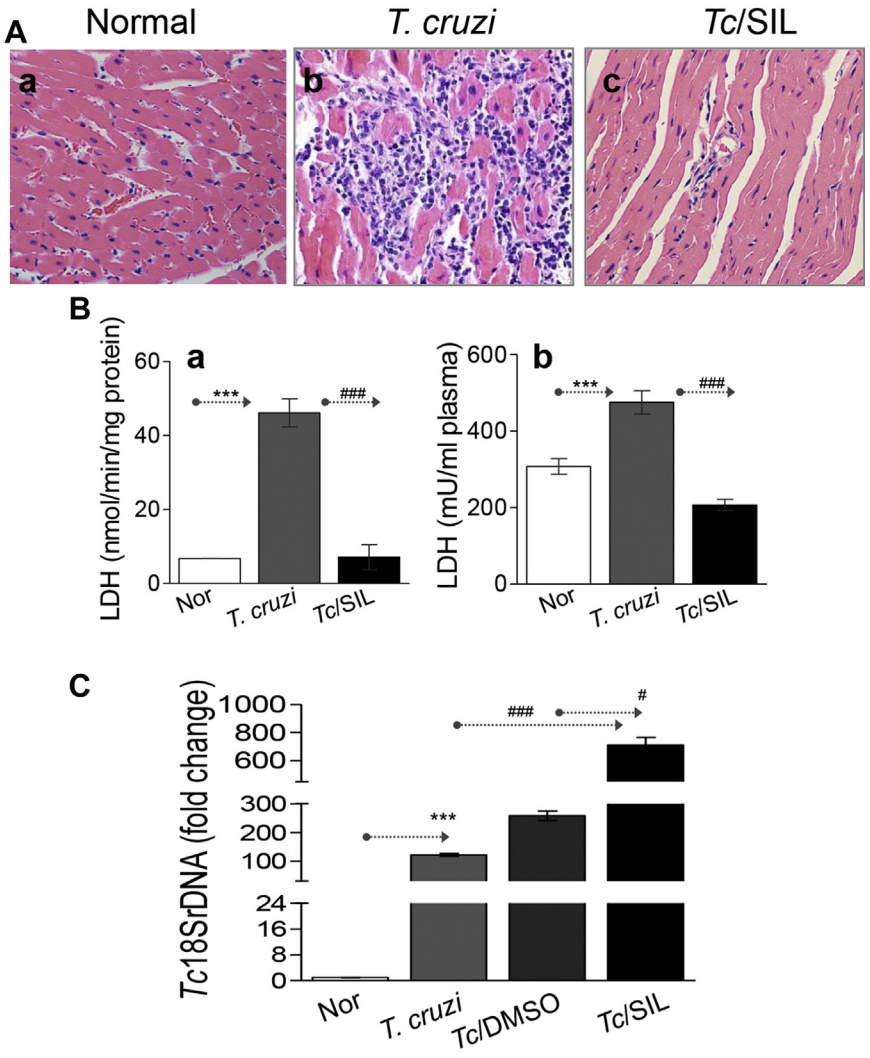

C57BL/6 mice were infected and treated with SIL as described in the text. Shown are **(A)** hematoxylin and eosin staining (**blue** = nuclear, **pink** = muscle/cytoplasm/keratin) of heart tissue sections at 150 days pi (magnification 20×). **(B)** The lactate dehydrogenase (LDH) activity in tissue homogenates **(a)** and plasma **(b)** was measured by spectrophotometry. **(C)** Myocardial parasite burden was determined by real-time quantitative PCR amplification of *Tc*18SrDNA sequence. Results were normalized to murine GAPDH DNA and presented as fold change in *Tc*DNA levels in chronically infected mice (±SIL). Abbreviations as in Figure 1.

carbonyl contents were increased by 2- to 3.5-fold in chronically infected/untreated (vs. normal) mice (Figure 4B, a-c) (all $^{*}p < 0.001_{ANOVA/Tukey}$). SIL treatment abolished the myocardial increase in mitochondrial ROS, LPO, and carbonyl contents, as well as plasma LPO content, in chagasic mice (Figures 4A and 4B) (all $^{\#}p < 0.001_{ANOVA/Tukey}$). These results, along with those presented in Figure 3, suggested that SIL treatment arrested the chronic oxidative adducts in chagasic myocardium, and these benefits were delivered by a mechanism independent of control of complex II-driven loss in coupled respiration.

SIL may have protective effects against oxidative stress by supporting an antioxidant system (30). Our data showed a 55% to 90% decline in GSK3β and MnSOD mRNA levels (Figure 5A, a and b) ($p < 0.001_{K\text{-}W/Dunn}$ and $p < 0.001_{ANOVA/Tukey}$ for panels a and b, respectively) and 68% decline in MnSOD activity (Figure 5B) ($^{*}p < 0.001_{ANOVA/Tukey}$) in the myocardium of chagasic (vs. normal) mice. The myocardial and plasma levels of total antioxidant

FIGURE 3 SIL Improved mtDNA-Encoded Gene Expression and Mitochondrial Respiration in Chagasic Mice

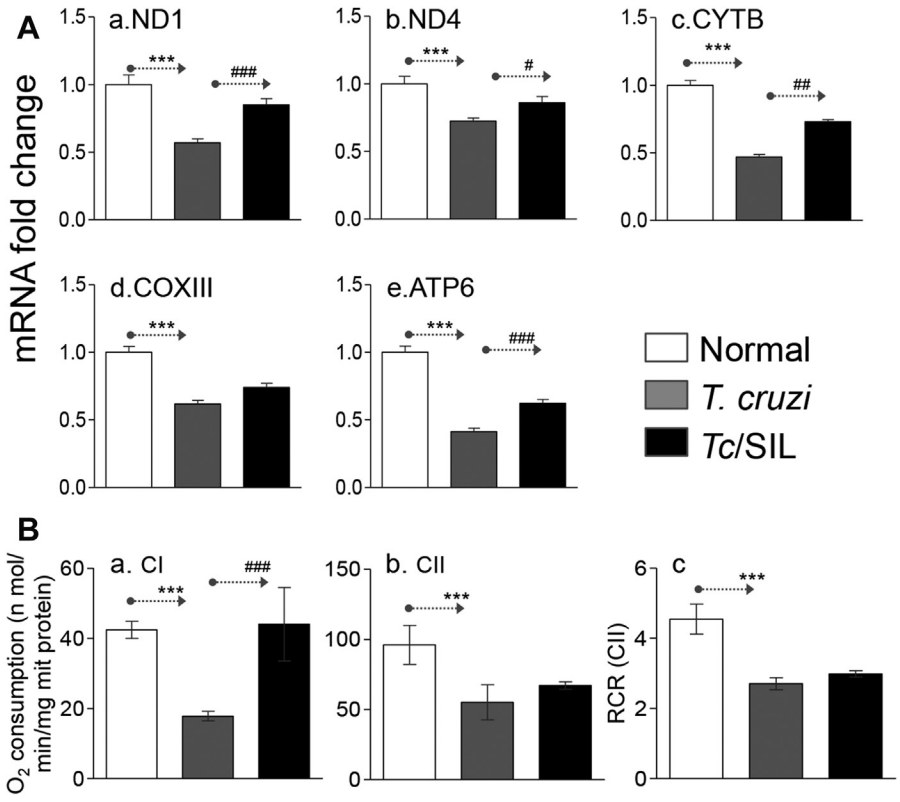

Mice were infected with *T. cruzi* and treated with SIL as described in the text. **(A)** Shown in **a–e** are the relative changes in gene expression for the mitochondrial DNA (mtDNA)-encoded genes *ND1*, *ND4*, *CYTB*, *COXIII*, and *ATP6*, determined by real-time quantitative RT-PCR. Results were normalized to GAPDH mRNA, and presented as fold change in mRNA levels in chronically infected mice (±SIL) as compared with that noted in normal control mice. **(B)** Cardiac mitochondria were isolated by differential centrifugation. Electron flow in freshly isolated mitochondria was supported with complex I (glutamate/pyruvate/malate, **a**) and complex II (succinate + rotenone, **b**) substrates and the ADP-stimulated state 3 respiration (i.e., oxygen consumption) was measured. Respiratory control ratio (RCR) **(c)** was calculated as the ratios between complex II–supported state 3 and state 4 rates. Abbreviations as in Figure 1.

capacity, determined as trolox units, was decreased by 74% and 45%, respectively, in chagasic mice (Figure 5C, a and b) (all $^{*}p < 0.001_{ANOVA/Tukey}$). When chagasic mice were treated with SIL, the myocardial antioxidant expression (GSK3β and MnSOD mRNAs) and MnSOD activity were only decreased by 20% and 10%, respectively, compared with that noted in normal mice (Figures 5A and 5B) (all $^{\#}p < 0.001_{ANOVA/Tukey\ or\ K\text{-}W/Dunn}$). The significant improvement in GSK3β mRNA level by SIL treatment was also observed when the median ± QR1 value was calculated (fold change 1.03 ± 1.15, 0.10 ± 0.17***, and 0.60 ± 0.12$^{\#\#\#}$ for normal, *Tc*-infected, and *Tc*-infected/SIL-treated, respectively, $^{*,\#}p < 0.001_{K\text{-}W/Dunn}$). Subsequently, SIL-treated chagasic mice exhibited normal levels of systemic and myocardial overall antioxidant capacity (Figure 5C) (all $^{\#}p < 0.001_{ANOVA/Tukey}$). These data suggested that SIL treatment enhanced the antioxidant capacity and allowed an oxidant/antioxidant balance in chagasic mice.

To confirm that SIL benefits were indeed delivered via regulating the antioxidant/oxidant balance, we used an in vitro system. Cardiac myocytes were infected with *T. cruzi* for 24 h, stained with intracellular probes, and then analyzed by fluorescence microscopy (Figure 6A). In response to *T. cruzi* infection, fluorescence of BCECF (detects normal pH) was decreased, whereas fluorescence of Fluo-4 (indicates Ca^{2+} overload), DCF (detects intracellular H_2O_2), and DHE (detects intracellular $O_2^{\bullet-}$) were increased in infected cardiac myocytes (Figure 6A, compare panels b, e, h, and k with a, d, g, and j). SIL treatment restored the normal intracellular pH, and partially decreased the *Tc*-induced increase in intracellular Ca^{2+} flux, and ROS generation in cardiac myocytes (Figure 6A, compare panels c, f, i, and l with b, e, h, and k). A

FIGURE 4 Oxidative Adducts in Chagasic Myocardium (±SIL)

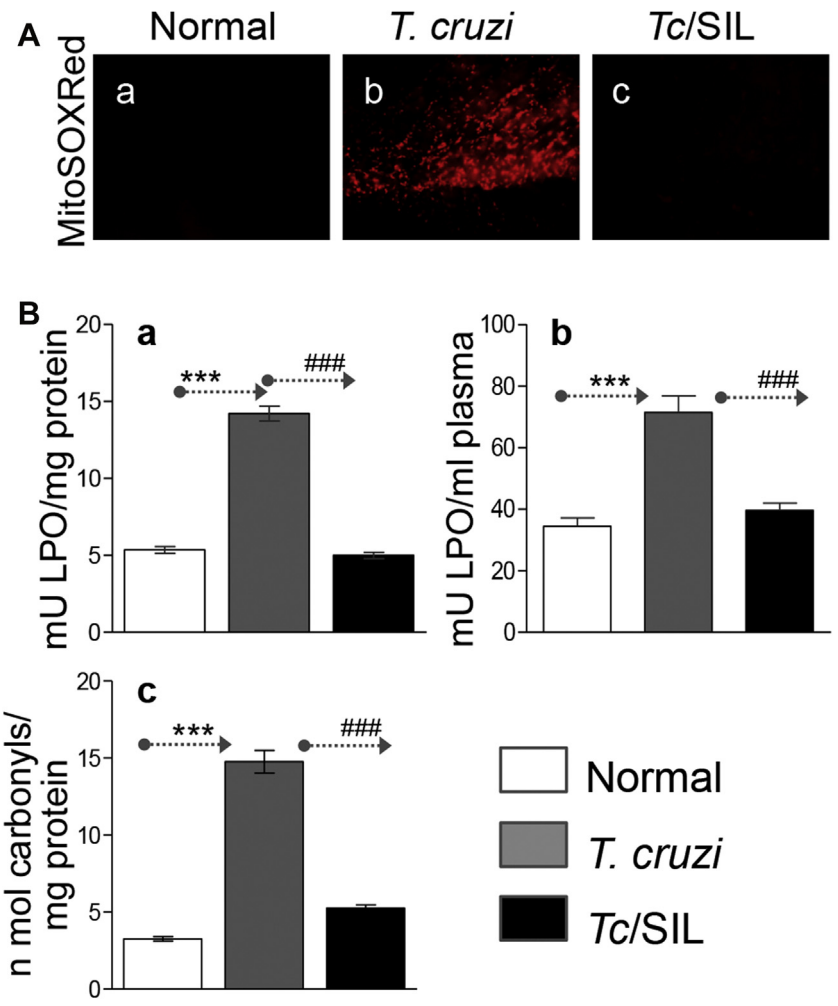

Mice were infected with *T. cruzi* and treated with SIL as described in the text. **(A)** Frozen heart tissue sections were incubated with MitoSOX Red (detects mitochondrial reactive oxygen species, fluoresces red) and imaged by fluorescence microscopy (magnification 20×). **(B)** Bar graphs show myocardial **(a)** and plasma **(b)** levels of lipid hydroperoxides (LPO) in chronically infected (±SIL) and control mice. **(c)** Myocardial protein carbonyls by an enzyme-linked immunosorbent assay. Abbreviations as in Figure 1.

quantitative evaluation of oxidative stress by Amplex red assay showed 7-fold and 3-fold increases in H_2O_2 release from infected/untreated and infected/SIL-treated cardiac myocytes, respectively, as compared with that noted in normal controls (Figure 6B) (all $^{*\#}p < 0.001_{ANOVA/Tukey}$). The NAD^+/NADH ratio reflects the metabolic activity and is an important component of redox state of cells. The NAD^+/NADH ratio (Figure 6C) and cell viability (Figure 6D) were decreased by 60% and 38%, respectively, in *Tc*-infected cardiac myocytes (all $^{*}p < 0.001_{ANOVA/Tukey}$), and treatment with SIL restored the normal NAD^+/NADH ratio and levels of cell viability in infected cells (Figures 6C and 6D) (all $^{\#}p < 0.001_{ANOVA/Tukey}$). Finally, to check whether the benefits of SIL in chronically *Tc*-infected mice would link the recovery of *Tc*-induced MnSOD decline, cardiac myocytes were transfected with pBI.EGFP or pBI.EGFP-MnSOD. Microscopic visualization of the total (Figure 6E, a) and GFP+ (Figure 6E, b) cells showed the transfection efficiency was ~72%. The pBI.EGFP-MnSOD-transfected cells exhibited a 60% decline in EGFP fluorescence in response to *T. cruzi* infection (Figure 6E, c) ($^{*}p < 0.001_{ANOVA/Tukey}$), and EGFP-MnSOD fluorescence was normalized to control levels in infected/SIL-treated cardiac myocytes (Figure 6E, c) ($^{\#}p < 0.001_{ANOVA/Tukey}$). Together, these data suggested that SIL benefits in preserving the redox

FIGURE 5 Myocardial Antioxidant Status in Chagasic Mice (±SIL)

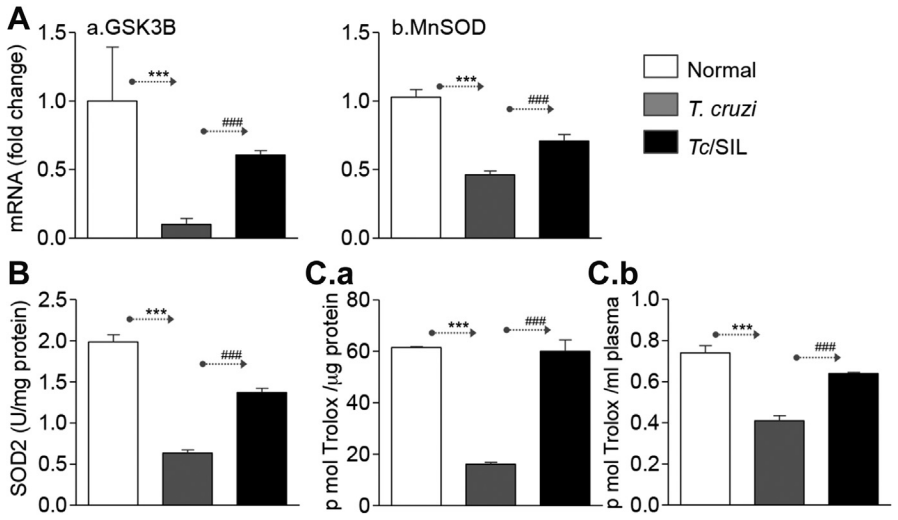

(A) Bar graphs show the mRNA levels for GSK3B **(a)** and MnSOD **(b)** antioxidants, determined by quantitative RT-PCR. Data were normalized to GAPDH mRNA. **(B)** MnSOD enzymatic activity in heart tissue homogenates of normal, chagasic, and chagasic/SIL-treated mice. **(C)** Shown are myocardial **(a)** and plasma **(b)** levels of total antioxidant capacity in normal and infected (±SIL) mice. Abbreviations as in Figure 1.

metabolic state and cellular health were delivered via preserving the antioxidant status that otherwise was compromised in response to *T. cruzi* infection.

DISCUSSION

In this study, we tested the hypothesis that the PDE5 inhibitor SIL would be beneficial in controlling the chronic CCM caused by *T. cruzi* infection. Our proposal was on the basis of the literature that NO/cGMP maintain cardiac homeostasis and inotropy via PKG1α activation (31), and PDE5 (catabolizes cGMP) is up regulated in hypertrophied heart (16,32). Mice infected with *T. cruzi* controlled the acute parasitemia within 45 days pi, but developed symptomatic CCC at >120 days pi (33). We used this therapeutic window of indeterminate phase for short-term treatment with SIL for 21 days, beginning day 45 pi. Our data showed a powerful protective effect of SIL against cardiac collagenosis and LV dysfunction in chagasic heart. The beneficial effects of SIL were not delivered via its direct effect on parasite persistence that is suggested to be the major cause for the development of chronic cardiomyopathy (reviewed in [34,35]). Instead, SIL inhibition of PDE5 prevented the loss in PKG1α activity, enhanced the overall antioxidant response and ROS scavenging capacity, and controlled the persistence of oxidative adducts and inflammatory infiltrate in chronic CCM. SIL treatment also controlled, at least partially, the ADP-coupled oxidative metabolism in chagasic myocardium. To the best of our knowledge, this is the first study demonstrating that SIL arrests the loss in antioxidant capacity and mitochondrial function and prevents the oxidative/inflammatory adducts that precipitate cardiomyocytes death and cardiac remodeling in CCM. We surmise that currently available PDE5 targeting drugs would potentially be useful for long-term health care of CCM patients.

The role of cGMP/PKG pathway and the therapeutic effect of PDE5 inhibitors have been well characterized in the pulmonary vasculature (36). The observation of increased expression of PDE5 in heart biopsies (or isolated primary cardiomyocytes) from patients exhibiting hypertrophy (37) and dilated or ischemic cardiomyopathy (38) fueled the research efforts investigating the benefits of PDE5 inhibitor in heart disease. Indeed, several studies in experimental models have demonstrated the beneficial effects of PDEF5 inhibitor in treating the acute ischemia/reperfusion-induced myocardial injury (21), pressure overload-induced cardiac hypertrophy (39), and heart failure of other etiologies. Recent studies have suggested the benefits of PDE5 inhibition in preserving the heart are delivered by decreasing the mitochondrial oxidative stress and increasing the antioxidant status in mice and cardiomyocytes (17–20).

C57BL/6 mice exhibit peak parasitemia during acute phase (14 to 35 days pi) (33). Myocardial

FIGURE 6 SIL Preserves the Oxidant/Antioxidant Balance in Cardiomyocytes Infected With *T. cruzi*

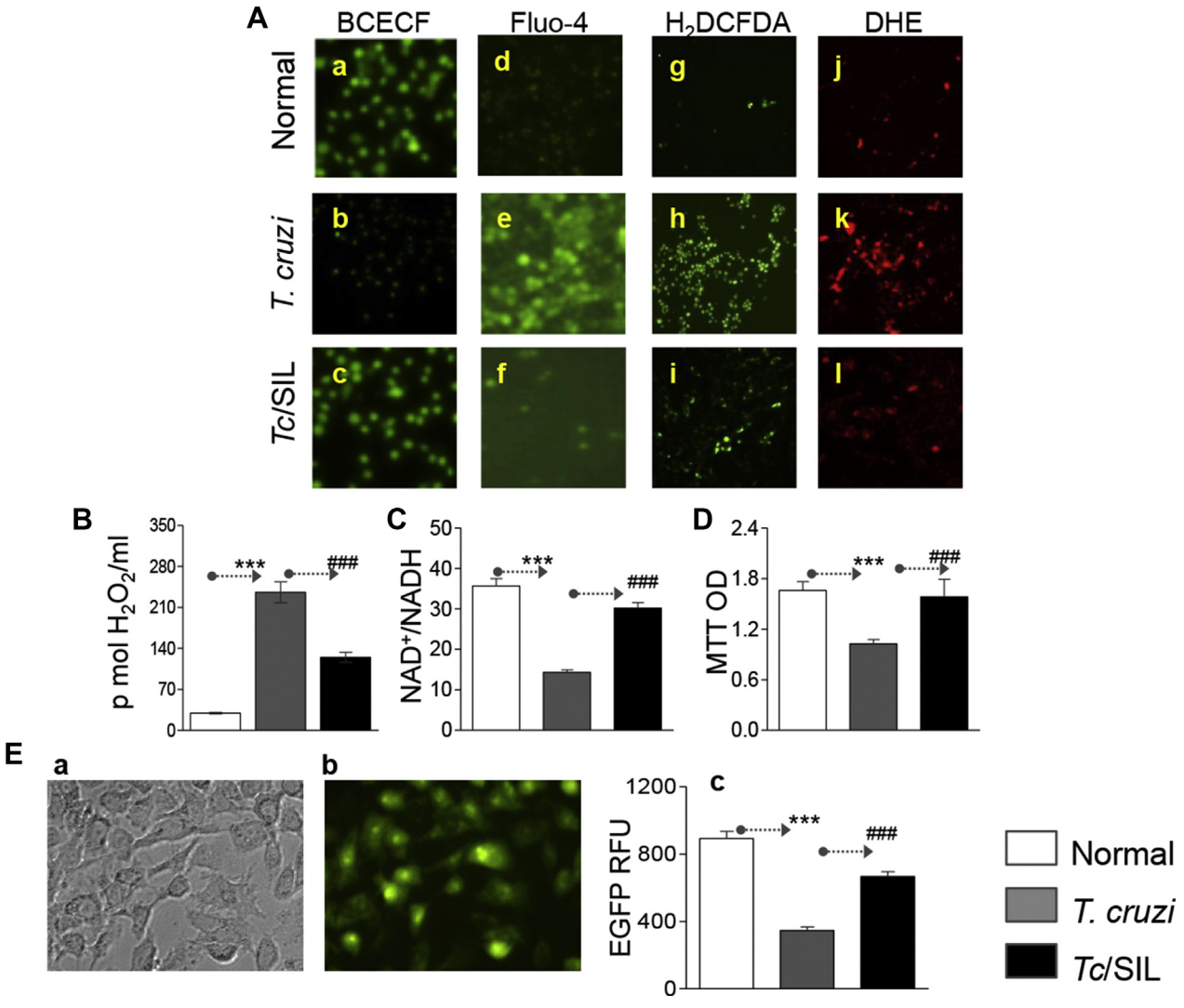

(A) Cardiac myocytes were infected with *T. cruzi* (cell/parasite ratio 1:5), and incubated for 24 h in the presence or absence of 10 nmol/l sildenafil. Cells were loaded with BCECF (fluoresces at normal pH, **a–c**), Fluo-4 (fluorescence shows intracellular Ca^{+2} level, **d–f**), H_2DCFDA (oxidized by intracellular reactive oxygen species [ROS] to fluorescent dichlorodihydrofluorescein [DCF], **g–i**), or DHE (oxidized by intracellular ROS to fluorescent ethidium, **j–l**). Shown are the representative images (magnification 40×), captured by fluorescence microscopy. **(B–D)** Cardiac myocytes were infected with *Tc* (±SIL). Bar graphs show **(B)** ROS release by an Amplex red assay, **(C)** NAD^+/NADH ratio, and **(D)** cell viability by MTT assay. **(E)** Cardiac myocytes were transfected with pBI.EGFP-MnSOD expression plasmid, infected with *T. cruzi*, and incubated in the presence or absence of sildenafil for 24 h. Bar graph shows MnSOD expression by EGFP-dependent fluorimetry. OD = optical density; RFU = relative fluorescence units; other abbreviations as in Figure 1.

remodeling, that is, increase in collagen isoforms and decline in *SERCA2* mRNA (Figure 1D), were prominent during the chronic phase that begun by ~120 days pi (33). Chronically infected chagasic mice developed LV systolic dysfunction evidenced by 42% to 55% decline in SV, cardiac output, and EF as is noted in chronically infected chagasic patients (Figure 1). Histological and molecular studies showed the infected mice showed cardiac collagenosis, extensive infiltration of inflammatory infiltrate and oxidative adducts in the heart that are hallmarks of CCM (Figure 1). Little is known about why echocardiographic parameters are altered in CCM; however, treatment with SIL provided enormous cardioprotective effects via preservation of LV systolic function in chagasic mice. Our findings of reduced LV wall thickness and cardiac fibrosis in SIL-treated mice may be indicative of a long-term, sustained improvement against CCM.

JACC: BASIC TO TRANSLATIONAL SCIENCE VOL. 1, NO. 4, 2016
JUNE 2016:235–50

We surmise that mice mimic the human development of clinical disease, and provided an excellent model system to demonstrate the therapeutic efficacy of SIL against CCM.

We and others have previously shown that *T. cruzi* invasion results in mitochondrial respiratory chain inefficiency and increased release of electrons to O_2 and $O_2^{\bullet-}$ production in cardiomyocytes (40) and chagasic hearts (24,41,42). PGC1-α is the master regulator of mitochondrial biogenesis (43,44), and indeed the mtDNA-encoded gene expression was normalized in the myocardium of chagasic mice by SIL treatment; and subsequently, SIL was effective in improving the complex I-driven electron gradient and ADP-coupled respiration (**Figure 3**). It is of note that mtDNA does not encode any of the subunits required for the assembly of complex II (45), and SIL had no beneficial impact in preserving the complex II-driven mitochondrial oxygen consumption in the chagasic heart (**Figure 3**). This observation suggests that mechanism(s) other than the compromise in mtDNA-encoded gene expression contribute to complex II-driven respiratory inefficiency in Chagas disease, to be delineated in future studies.

Despite the continuation of the loss in CII complex driven respiration, SIL treatment was effective in attenuating the *Tc*-induced mitochondrial ROS, myocardial oxidative adducts (protein carbonyls and LPO), and cell death (**Figure 4**). Chronic oxidative stress is shown to correlate with increased expression of PDE5 in myocytes during chronic heart failure (46), though the physiological or mechanistic relevance of PDE5 in aggravating oxidative stress is unknown. Likewise, it is not known whether control of oxidative damage by PDE5 inhibitor is causatively related with cGMP/PKG activation. Yet, increase in cGMP can inhibit NADPH oxidase expression/activity, thereby reducing $O_2^{\bullet-}$ production (47). Our in vitro and in vivo studies suggested that PDE5 was at the nexus of compromised antioxidant response, and SIL treatment enhanced the ROS scavenging capacity by activation of MnSOD expression and activity (**Figures 5 and 6**); and thereby the underlying cause for oxidant/antioxidant imbalance in response to *T. cruzi* infection. The potential advantage of a therapeutic approach on the basis of inhibition of PDE5 appears to be the host's ability to avoid risks associated with excessive $O_2^{\bullet-}$ and •NO that lead to overproduction of a highly stable, peroxynitrite-free radical. Further studies will be required to elucidate whether PDE5 suppresses the antioxidant capacity via targeting the PGC-1-α/NRF2 pathway of antioxidant response in the heart.

A recent study showed that *T. cruzi* signals both TGF-β-dependent and -independent fibrotic pathways in cardiac myocytes (9), providing evidence for the role of the parasite in eliciting cardiac hypertrophy. The current published reports also accept that parasite persistence is the main cause for chronic cardiac inflammation, cardiomyocytes' injury and death, and myofibroblasts' involvement in cardiac remodeling in Chagas disease (reviewed in [48]). However, in this study, SIL-treated/infected mice exhibited an increase in tissue parasite burden when compared with that noted in untreated/infected mice, and still controlled the collagenosis, oxidative and inflammatory stress, and LV dysfunction. These data suggested that parasite persistence is not the sole cause for continuance of injurious processes in the heart. Indeed, intracellular proteins (e.g., myosin) that are exposed to immune system due to cardiomyocyte injuries are shown to sustain chronic activation of T-cell responses in Chagas disease (49–51). We have found that post-translational oxidative modifications of cardiac proteins generated neoantigens that were recognized by serum antibodies in chagasic patients, and this response paralleled with the pathological events during Chagas disease development (52). Treatment of infected rodents with chemical antioxidant provided a significant control of cardiac remodeling and antibody cytotoxicity directed against cardiac proteins (12). Thus, we surmise that besides parasite persistence, host factors (e.g., oxidative stress, oxidized antigens) play an important role in chronic inflammation in Chagas disease, and cardioprotective effects of SIL were delivered via preserving the oxidant/antioxidant balance and limiting the nonspecific immune activation in the chagasic host.

A novel observation in this study was that *T. cruzi* infection decreased the expression of *SERCA2*. *SERCA2* is a Ca^{2+} ATPase that transfers Ca^{2+} from the cytosol of the cell to the lumen of the sarcoplasmic reticulum at the expense of ATP hydrolysis during muscle relaxation (53). Several studies have suggested the *SERCA2*/endoplasmic reticulum (ER) stress dysregulates the intracellular Ca^{2+} cycling and contributes to the risk of future heart failure events (54). It is shown that induction of ER stress in human heart failure was significantly correlated with increased myocardial PDE5 expression, and SIL treatment reduced the ER stress and corresponding cell apoptosis in isoprenaline-induced heart failure; studies in cultured cardiomyocytes showed similar results (55). Our finding of improved *SERCA2* expression in SIL-treated chagasic mice and Ca^{+2} handling in *Tc*-infected/SIL-treated cardiomyocytes provide further evidence that PDE5 inhibition in heart failure might contribute to attenuation of ER stress through increased SERCA activity and restoration of intracellular Ca^{2+}balance.

Although several studies have shown increased expression of PDE5 in diseased heart and the benefits of PDE5 inhibitors in improving heart failure with lower ejection fraction, several controversies remain. Some investigators have noted no increase in hypertrophy upon deletion of cGMP/PKG in cardiomyocytes (56), whereas others have suggested that PDE5 expression in normal heart and in cardiac biopsies of mammalian models of heart failure as well as in humans with heart failure occur at a very low level (57), and the effects of SIL on cGMP hydrolysis in experimental models of ischemia/perfusion were likely through inhibition of PDE1 (along with PDE5) (58). A recently concluded randomized clinical trial of heart failure patients with preserved ejection fraction (>50%) showed no significant beneficial effect of SIL in improving the exercise capacity or clinical status. Clearly, large randomized trials with careful documentation and analysis of effects of PDE5 inhibitors on micro and macro parameters of heart pathology and physiology will be required before the use of PDE5 inhibitors for management of heart disease can be clinically implemented.

CONCLUSIONS

In summary, our findings provide the first evidence that SIL has a powerful cardioprotective effect against cardiac collagenosis and LV dysfunction in chagasic disease. SIL inhibition of PDE5 enhanced the overall antioxidant response and ROS scavenging capacity, and controlled the chronic oxidative and inflammatory stress in chagasic heart. SIL treatment also restored, at least partially, the mitochondrial oxidative metabolism in chagasic myocardium. These results provide us impetus to test the potential efficacy of available PDE5 targeting drugs in other animal models of Chagas disease, and subsequently, in chagasic patients.

REPRINT REQUEST AND CORRESPONDENCE: Dr. Nisha Jain Garg, Department of Microbiology and Immunology, University of Texas Medical Branch, 301 University Boulevard, Galveston, Texas 77555-1070. E-mail: nigarg@utmb.edu. OR Dr. Jian-jun Wen, Department of Microbiology and Immunology, 3.152 Medical Research Building, University of Texas Medical Branch, 301 University Boulevard, Galveston, Texas 77555-1070. E-mail: jiawen@utmb.edu.

PERSPECTIVES

COMPETENCY IN MEDICAL KNOWLEDGE: *Trypanosoma cruzi* protozoan parasite remain the most common cause of nonischemic cardiomyopathy (called Chagas disease) in Latin America. A recent prospective, multicenter randomized study involving >2,800 patients with Chagas cardiomyopathy who received benznidazole (antiparasite drug) or placebo concluded that treatment with antiparasite drug provided no significant benefit in reducing the cardiac clinical deterioration through 5 years of follow-up. There is no specific treatment available to control the progressive cardiomyopathy in chagasic patients. Current literature suggests that nitric oxide and cGMP maintain cardiac homeostasis and inotropy via cGMP-dependent protein kinase (PKG1α) activation, and PDE5 (catabolizes cGMP) is upregulated in hypertrophy conditions. Thus, we examined the therapeutic efficacy of PDE5 inhibitor (sildenafil) in a murine model of Chagas disease. Sildenafil treatment during a therapeutic window (i.e., after control of acute parasitemia but before development of cardiomyopathy) had a powerful cardioprotective effect against cardiac collagenosis and left ventricular dysfunction in chagasic disease.

TRANSLATIONAL OUTLOOK: Currently available PDE5 targeting drugs would potentially be useful for long-term health care of chagasic cardiomyopathy patients.

REFERENCES

1. World Health Organization. Chagas Disease: Control and Elimination: Report of the Secretariat. Geneva, Switzerland: UNDP/World Bank/WHO, 2010. Available at: http://apps.who.int/gb/ebwha/pdf_files/WHA63/A63_17-en.pdf. Accessed April 4, 2016.

2. Cantey PT, Stramer SL, Townsend RL, et al. The United States Trypanosoma cruzi Infection Study: evidence for vector-borne transmission of the parasite that causes Chagas disease among United States blood donors. Transfusion 2012;52:1922–30.

3. Bern C, Montgomery SP. An estimate of the burden of Chagas disease in the United States. Clin Infect Dis 2009;49:e52–4.

4. Gascon J, Bern C, Pinazo MJ. Chagas disease in Spain, the United States and other non-endemic countries. Acta Trop 2010;115:22–7.

5. Bern C, Kjos S, Yabsley MJ, Montgomery SP. Trypanosoma cruzi and Chagas' disease in the United States. Clin Microbiol Rev 2011;24:655–81.

6. Rassi A Jr., Rassi A, Marin-Neto JA. Chagas disease. Lancet 2010;375:1388–402.

7. Hidalgo R, Marti-Carvajal AJ, Kwong JS, Simancas-Racines D, Nicola S. Pharmacological interventions for treating heart failure in patients with chagas cardiomyopathy. Cochrane Database Syst Rev 2012;11:CD009077.

8. Lee BY, Bacon KM, Bottazzi ME, Hotez PJ. Global economic burden of Chagas disease: a computational simulation model. Lancet Infect Dis 2013;13:342–8.

9. Udoko AN, Johnson CA, Dykan A, et al. Early regulation of profibrotic genes in primary human cardiac myocytes by Trypanosoma cruzi. PLoS Negl Trop Dis 2016;10:e0003747.

10. Tanowitz HB, Machado FS, Spray DC, et al. Developments in the management of chagasic cardiomyopathy. Expert Rev Cardiovasc Ther 2015;13:1393–409.

11. Gupta S, Wen JJ, Garg NJ. Oxidative stress in Chagas disease. Interdiscip Perspect Infect Dis 2009;2009:190354.

12. Wen J-J, Gupta S, Guan Z, et al. Phenyl-alpha-tert-butyl-nitrone and benzonidazole treatment controlled the mitochondrial oxidative stress and evolution of cardiomyopathy in chronic chagasic rats. J Am Coll Cardiol 2010;55:2499–508.

13. Dhiman M, Wan X-X, Popov VL, Vargas G, Garg NJ. MnSOD^{tg} mice control myocardial inflammatory and oxidative stress and remodeling responses elicited in chronic Chagas disease. J Am Heart Assoc 2013;2:e000302.

14. Tsai EJ, Kass DA. Cyclic GMP signaling in cardiovascular pathophysiology and therapeutics. Pharmacol Ther 2009;122:216–38.

15. Layland J, Li JM, Shah AM. Role of cyclic GMP-dependent protein kinase in the contractile response to exogenous nitric oxide in rat cardiac myocytes. J Physiol 2002;540:457–67.

16. Takimoto E. Cyclic GMP-dependent signaling in cardiac myocytes. Circ J 2012;76:1819–25.

17. Zhang M, Kass DA. Phosphodiesterases and cardiac cGMP: evolving roles and controversies. Trends Pharmacol Sci 2011;32:360–5.

18. Lee DI, Kass DA. Phosphodiesterases and cyclic GMP regulation in heart muscle. Physiology (Bethesda) 2012;27:248–58.

19. Nagayama T, Zhang M, Hsu S, Takimoto E, Kass DA. Sustained soluble guanylate cyclase stimulation offsets nitric-oxide synthase inhibition to restore acute cardiac modulation by sildenafil. J Pharmacol Exp Ther 2008;326:380–7.

20. Seya K, Ono K, Fujisawa S, Okumura K, Motomura S, Furukawa K. Cytosolic Ca2+-induced apoptosis in rat cardiomyocytes via mitochondrial NO-cGMP-protein kinase G pathway. J Pharmacol Exp Ther 2013;344:77–84.

21. Salloum FN, Abbate A, Das A, et al. Sildenafil (Viagra) attenuates ischemic cardiomyopathy and improves left ventricular function in mice. Am J Physiol Heart Circ Physiol 2008;294:H1398–406.

22. Bhan A, Sirker A, Zhang J, et al. High-frequency speckle tracking echocardiography in the assessment of left ventricular function and remodeling after murine myocardial infarction. Am J Physiol Heart Circ Physiol 2014;306:H1371–83.

23. Dhiman M, Garg NJ. NADPH oxidase inhibition ameliorates Trypanosoma cruzi-induced myocarditis during Chagas disease. J Pathol 2011;225:583–96.

24. Wen JJ, Garg NJ. Mitochondrial generation of reactive oxygen species is enhanced at the Q(o) site of the complex III in the myocardium of Trypanosoma cruzi-infected mice: beneficial effects of an antioxidant. J Bioenerg Biomembr 2008;40:587–98.

25. Sen T, Sen N, Noordhuis MG, et al. OGDHL is a modifier of AKT-dependent signaling and NF-kappaB function. PLoS One 2012;7. e48770.

26. Garg NJ, Popov VL, Papaconstantinou J. Profiling gene transcription reveals a deficiency of mitochondrial oxidative phosphorylation in Trypanosoma cruzi-infected murine hearts: implications in chagasic myocarditis development. Biochim Biophys Acta 2003;1638:106–20.

27. Gupta S, Garg NJ. TcVac3 induced control of Trypanosoma cruzi infection and chronic myocarditis in mice. PLoS One 2013;8:e59434.

28. Wen J-J, Garg NJ. Mitochondrial complex III defects contribute to inefficient respiration and ATP synthesis in the myocardium of Trypanosoma cruzi-infected mice. Antioxid Redox Signal 2010;12:27–37.

29. Davies MJ. Protein oxidation and peroxidation. Biochem J 2016;473:805–25.

30. Sheweita S, Salama B, Hassan M. Erectile dysfunction drugs and oxidative stress in the liver of male rats. Toxicol Rep 2015;2:933–8.

31. Hammond J, Balligand JL. Nitric oxide synthase and cyclic GMP signaling in cardiac myocytes: from contractility to remodeling. J Mol Cell Cardiol 2012;52:330–40.

32. Takahashi K, Osanai T, Nakano T, Wakui M, Okumura K. Enhanced activities and gene expression of phosphodiesterase types 3 and 4 in pressure-induced congestive heart failure. Heart Vessels 2002;16:249–56.

33. Garg NJ, Bhatia V, Gerstner A, DeFord J, Papaconstantinou J. Gene expression analysis in mitochondria from chagasic mice: alterations in specific metabolic pathways. Biochemical J 2004;381:743–52.

34. Nagajyothi F, Machado FS, Burleigh BA, et al. Mechanisms of Trypanosoma cruzi persistence in Chagas disease. Cell Microbiol 2012;14:634–43.

35. Machado FS, Tyler KM, Brant F, Esper L, Teixeira MM, Tanowitz HB. Pathogenesis of Chagas disease: time to move on. Front Biosci (Elite Ed) 2012;4:1743–58.

36. Pabani S, Mousa SA. Current and future treatment of pulmonary hypertension. Drugs Today (Barc) 2012;48:133–47.

37. Nagendran J, Archer SL, Soliman D, et al. Phosphodiesterase type 5 is highly expressed in the hypertrophied human right ventricle, and acute inhibition of phosphodiesterase type 5 improves contractility. Circulation 2007;116:238–48.

38. Shan X, Quaile MP, Monk JK, French B, Cappola TP, Margulies KB. Differential expression of PDE5 in failing and nonfailing human myocardium. Circ Heart Fail 2012;5:79–86.

39. Takimoto E, Champion HC, Li M, et al. Chronic inhibition of cyclic GMP phosphodiesterase 5A prevents and reverses cardiac hypertrophy. Nat Med 2005;11:214–22.

40. Gupta S, Bhatia V, Wen J-J, Wu Y, Huang M-H, Garg NJ. Trypanosoma cruzi infection disturbs mitochondrial membrane potential and ROS production rate in cardiomyocytes. Free Radic Biol Med 2009;47:1414–21.

41. Vyatkina G, Bhatia V, Gerstner A, Papaconstantinou J, Garg NJ. Impaired mitochondrial respiratory chain and bioenergetics during chagasic cardiomyopathy development. Biochim Biophys Acta 2004;1689:162–73.

42. Wen J-J, Yachelini PC, Sembaj A, Manzur RE, Garg NJ. Increased oxidative stress is correlated with mitochondrial dysfunction in chagasic patients. Free Radic Biol Med 2006;41:270–6.

43. Puigserver P, Spiegelman BM. Peroxisome proliferator-activated receptor-gamma coactivator 1 alpha (PGC-1 alpha): transcriptional coactivator and metabolic regulator. Endocr Rev 2003;24:78–90.

44. Bensinger SJ, Tontonoz P. Integration of metabolism and inflammation by lipid-activated nuclear receptors. Nature 2008;454:470–7.

45. Marin-Garcia J, Ananthakrishnan R, Goldenthal MJ. Heart mitochondrial DNA and enzyme changes during early human development. Mol Cell Biochem 2000;210:47–52.

46. Lu Z, Xu X, Hu X, et al. Oxidative stress regulates left ventricular PDE5 expression in the failing heart. Circulation 2010;121:1474–83.

47. Koupparis AJ, Jeremy JY, Muzaffar S, Persad R, Shukla N. Sildenafil inhibits the formation of superoxide and the expression of gp47 NAD[P]H oxidase induced by the thromboxane A2 mimetic, U46619, in corpus cavernosal smooth muscle cells. BJU Int 2005;96:423–7.

48. Gutierrez FR, Guedes PM, Gazzinelli RT, Silva JS. The role of parasite persistence in pathogenesis of Chagas heart disease. Parasite Immunol 2009;31:673–85.

49. Leon JS, Godsel LM, Wang K, Engman DM. Cardiac myosin autoimmunity in acute chagas' heart disease. Infect Immun 2001;69:5643–9.

50. Leon JS, Daniels MD, Toriello KM, Wang K, Engman DM. A cardiac myosin-specific autoimmune response is induced by immunization with Trypanosoma cruzi proteins. Infect Immun 2004;72:3410–7.

51. Bonney KM, Engman DM. Chagas heart disease pathogenesis: one mechanism or many? Curr Mol Med 2008;8:510–8.

52. Dhiman M, Zago MP, Nunez S, Nunez-Burgio F, Garg NJ. Cardiac oxidized antigens are targets of immune recognition by antibodies and potential molecular determinants in Chagas disease pathogenesis. Plos One 2012;7. e28449.

53. Vangheluwe P, Raeymaekers L, Dode L, Wuytack F. Modulating sarco(endo)plasmic reticulum Ca2+ ATPase 2 (SERCA2) activity: cell biological implications. Cell Calcium 2005;38:291–302.

54. Kraus WE, Muoio DM, Stevens R, et al. Metabolomic quantitative trait loci (mQTL) mapping implicates the ubiquitin proteasome system in cardiovascular disease pathogenesis. PLoS Genet 2015;11:e1005553.

55. Gong W, Duan Q, Cai Z, et al. Chronic inhibition of cGMP-specific phosphodiesterase 5 suppresses endoplasmic reticulum stress in heart failure. Br J Pharmacol 2013;170:1396–409.

56. Patrucco E, Domes K, Sbroggio M, et al. Roles of cGMP-dependent protein kinase I (cGKI) and PDE5 in the regulation of Ang II-induced cardiac hypertrophy and fibrosis. Proc Natl Acad Sci U S A 2014;111:12925–9.

57. Degen CV, Bishu K, Zakeri R, Ogut O, Redfield MM, Brozovich FV. The emperor's new clothes: PDE5 and the heart. PLoS One 2015;10:e0118664.

58. Vandeput F, Krall J, Ockaili R, et al. cGMP-hydrolytic activity and its inhibition by sildenafil in normal and failing human and mouse myocardium. J Pharmacol Exp Ther 2009;330:884–91.

KEY WORDS antioxidant/oxidant balance, chagasic cardiomyopathy, chronic inflammation, LV function, mitochondrial respiration, sildenafil, *Trypanosoma cruzi*